J Mol Model (2013) 19:2225–2234
DOI 10.1007/s00894-013-1772-5

ORIGINAL PAPER

Theoretical investigation of Co(0)-catalyzed intramolecular hydroacylation of 4-pentenal

Qingxi Meng · Fen Wang · Ming Li

Received: 21 October 2012 / Accepted: 14 January 2013 / Published online: 31 January 2013

Abstract Density functional theory (DFT) was used to investigate cobalt(0)-catalyzed intramolecular hydroacylation of 4-pentenal. The calculated results indicated the involvement of five possible reaction pathways: the formation of cyclopentanone, cyclobutanone, butylenes, cyclobutane, and cyclopropane, respectively. The former two are pathways of Co(0)-catalyzed intramolecular hydroacylation, while the latter three are pathways of decarbonylation. The formation of cyclopentanone was the most favorable channel, and the oxidative addition reaction of 4-pentenal was the rate-determining step. Hence, the dominant product predicted theoretically was cyclopentanone, which was consistent with experimental results. Solvation had a significant effect, and greatly decreased the free energies of all intermediates and transition states.

Keywords Cobalt(0)-catalyzed intramolecular hydroacylation · 4-pentenal · Reaction mechanism · DFT

Introduction

Transition metal-catalyzed C–H bond activation has received considerable attention in synthetic organic chemistry as the cleavage of an unreactive C–H bond and subsequent addition of the C–H unit into unsaturated substrates such as alkenes and alkynes could lead to the formation of new C–C bonds [1–6]. During the last two decades, many successful applications of catalytic C–H bond activation directed toward the construction of C–C bonds have been reported in the synthetic community [7], with C–C bond-forming reactions via C–H bond activation being the focus of extensive study in the fields of organic and organometallic chemistry [6–9].

The intramolecular and intermolecular hydroacylation of alkenes or alkynes catalyzed by transition metals is one of the most useful C–H bond activation processes [10]. Many transition metals, such as Rh [11–18], Co [19–24], Ni [25, 26], Ru [27, 28], and Ir [29], have been found to be able to catalyze such hydroacylation.

Morehead et al. [30] studied the mechanism of rhodium-catalyzed intramolecular hydroacylation of alkenes theoretically using the software package DMol3 and the two-layer ONIOM approach [(B3LYP/LANL2DZ: UFF) method], and proved that reductive elimination was the rate-limiting step. Wu et al. [31] reported rhodium-catalyzed intramolecular hydroacylation of 4-alkynals for a model system using MP2 calculations, and thought that the oxidative addition of aldehydes was the rate-determining step. We reported the intermolecular hydroacylation of an ethene- or ethyne-acetaldehyde-$[Rh(PH_3)_2]^+$ model system at the B3LYP/6–311++G(d,p) level [LANL2DZ(f) for Rh and P] [32]. Recently, we studied the intermolecular hydroacylation of vinylsilane and benzaldehyde catalyzed by the rhodium(I) olefin complex at the B3LYP/6–31 G(d,p) level [LANL2DZ (f) for Rh], and speculated that the carbonyl rearrangement is of great importance and that the use of the cyclopentadienyl ligand with electron-withdrawing groups decreased the reaction free energies [33].

Vinogradov and co-workers [19–21] studied experimentally cobalt(0)-catalyzed intramolecular hydroacylation of 4-pentenal (Scheme 1), and suggested a likely mechanism.

Electronic supplementary material The online version of this article (doi:10.1007/s00894-013-1772-5) contains supplementary material, which is available to authorized users.

Q. Meng (✉)
College of Chemistry and Material Science, Shandong Agricultural University, Taian, Shandong 271018, People's Republic of China
e-mail: qingxim@sdau.edu.cn

F. Wang
Department of Chemistry, Taishan University, Taian, Shandong 271021, People's Republic of China

M. Li
College of Chemistry and Chemical Engineering, Southwest University, Chongqing 400715, People's Republic of China

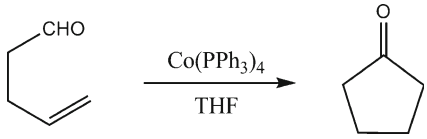

Scheme 1 Cobalt(0)-catalyzed intramolecular hydroacylation of 4-pentenal

They showed that the dominant product was cyclopentanone. In order to understand in detail the reaction mechanism of the intramolecular hydroacylation catalyzed by cobalt complexes, Co(0)-catalyzed intramolecular hydroacylation of 4-pentenal was studied in the present work. The possible reaction mechanisms are outlined in Scheme 2.

Computational details

All calculations were carried out with the Gaussian 03 program suite [34]. The geometries of all species were fully optimized with density functional theory (DFT) [35] using B3LYP method [36, 37]. The 6–31 G(d,p) basis set was used for all atoms. Frequency calculations at the same level were performed to confirm each stationary point to be either a minimum (**M**) or a transition structure (**T**). The transition states were verified by intrinsic reaction coordinate (IRC) calculations [38] and by animating the negative eigenvector coordinates with a visualization program (Molekel 4.3) [39, 40]. The bonding characteristics were analyzed by natural bond orbital (NBO) theory [41–44]. NBO analysis was performed by utilizing NBO5.0 code [45] with the optimized structures. Based on the gas phase optimized geometry for each species, the solvent effects of THF (tetrahydrofuran, ε=7.58) were studied by performing a self-consistent reaction field (SCRF) [46, 47] of polarizable continuum model (PCM) [48] approach at the same computational level using the default parameters except temperature (393.15 Kelvin was used).

In addition, the electron densities ρ at the bond critical points (BCPs) or the ring critical points (RCPs) for some species were calculated by employing the AIM 2000 program package [49, 50].

Results and discussion

The relative free energies, ΔG(sol), including solvent energies, and the relative gas phase free energies, ΔG, enthalpies, ΔH, and zero-point energy (ZPE) corrected electronic energies, ΔE, are summarized in Tables S1 and S2. Reaction free energy barriers, $\Delta G^{\neq}$(sol) (kJ mol^{-1}) (in solvent) and $\Delta G^{\neq}$ (kJ mol^{-1}) (in gas phase), reaction enthalpy barriers, $\Delta H^{\neq}$ (kJ mol^{-1}), and reaction energy barriers, $\Delta E^{\neq}$ (kJ mol^{-1}), for the transition states were shown in Table 1. Unless otherwise noted, the discussed energies were relative free energies, ΔG(sol), or reaction free energy barriers, $\Delta G^{\neq}$(sol), in the following discussion.

The complexation reaction of $Co(PMe_3)_4$ and 4-pentenal

As illustrated in Scheme 2, the complexation reaction of Co$(PMe_3)_4$ and 4-pentenal resulted in two possible Co$(PMe_3)_2$(4-pentenal) complexes: **M1a** and **M1b**. NBO analysis showed that **M1a** and **M1b** involved two back-donation π bonds between cobalt and C1–O, C4–C5 double bonds of 4-pentenal. The occupied π_{C1-O} or π_{C4-C5} orbital of 4-pentenal acted on the empty hybrid orbital of cobalt leading to the σ coordinate bond; on the other hand, the occupied d orbital (d_{xy}, d_{xz}, d_{yz}) of cobalt acted on the empty π^*_{C1-O} or π^*_{C4-C5} orbital of 4-pentenal leading to the back-donation π bond. Obviously, the formation of the back-donation π bond lowered the system's energy and would help to stabilize **M1a** and **M1b**. Both the geometric isomers **M1a** and **M1b** were tetrahedral in structure, and thus the difference was the relative spatial position of cobalt, C1–O and C4–C5 double bonds. The Co–O, Co–C1, Co–C4, Co–C5 bonds were 1.908, 1.981, 2.096, 2.150 Å for **M1a**, 2.047, 2.035, 2.010, 1.999 Å for **M1b**, respectively.

Of these two complexes, **M1a** was calculated to the more stable, by 25.2 kJ mol^{-1}, suggesting that it was more likely to exist. In **M1a**, the NBO energy of the C1–H1 bond was lower than 4-pentenal by 147 kJ mol^{-1}, and the NBO energy of the C1–H1 bond of **M1b** was lower than that of 4-pentenal by 113 kJ mol^{-1}. Hence, in **M1a** and **M1b**, formation of the back-donation π bond weakened and activated C1–H1 bonds, which resulted in the oxidative addition of 4-pentenal.

Formation of cyclopentanone

Figure 1 showed the potential energy hypersurface for the pathway forming cyclopentanone. Intermediate **M1a** underwent the C–H oxidative addition reaction through transition state **T1a** with a reaction free energy barrier of 68.4 kJ mol^{-1} to generate the five-coordinated complex **M2a**. Then, **M2a** went through a hydrogen transfer reaction via transition state **T2a** with a reaction free energy barrier of 49.2 kJ mol^{-1}, leading to the complex **M3a**. Finally, **M3a** underwent a reductive elimination reaction via transition state **T3a** with a reaction free energy barrier of 50.3 kJ mol^{-1} to form the complex **M4a**, yielding the cyclopentanone **P1**. Clearly, the oxidative addition reaction of 4-pentenal was the rate-determining step for this reaction channel.

In $\sigma_{(Co-H1)}$ bond formation, as illustrated in Fig. 2, the distance between C1 and H1, $d_{(C1-H1)}$, increased, $d_{(Co-H1)}$ decreased, and Co shifted to C1. It was clear that a significant interaction between Co and H1 occurred, and that the C1–H1

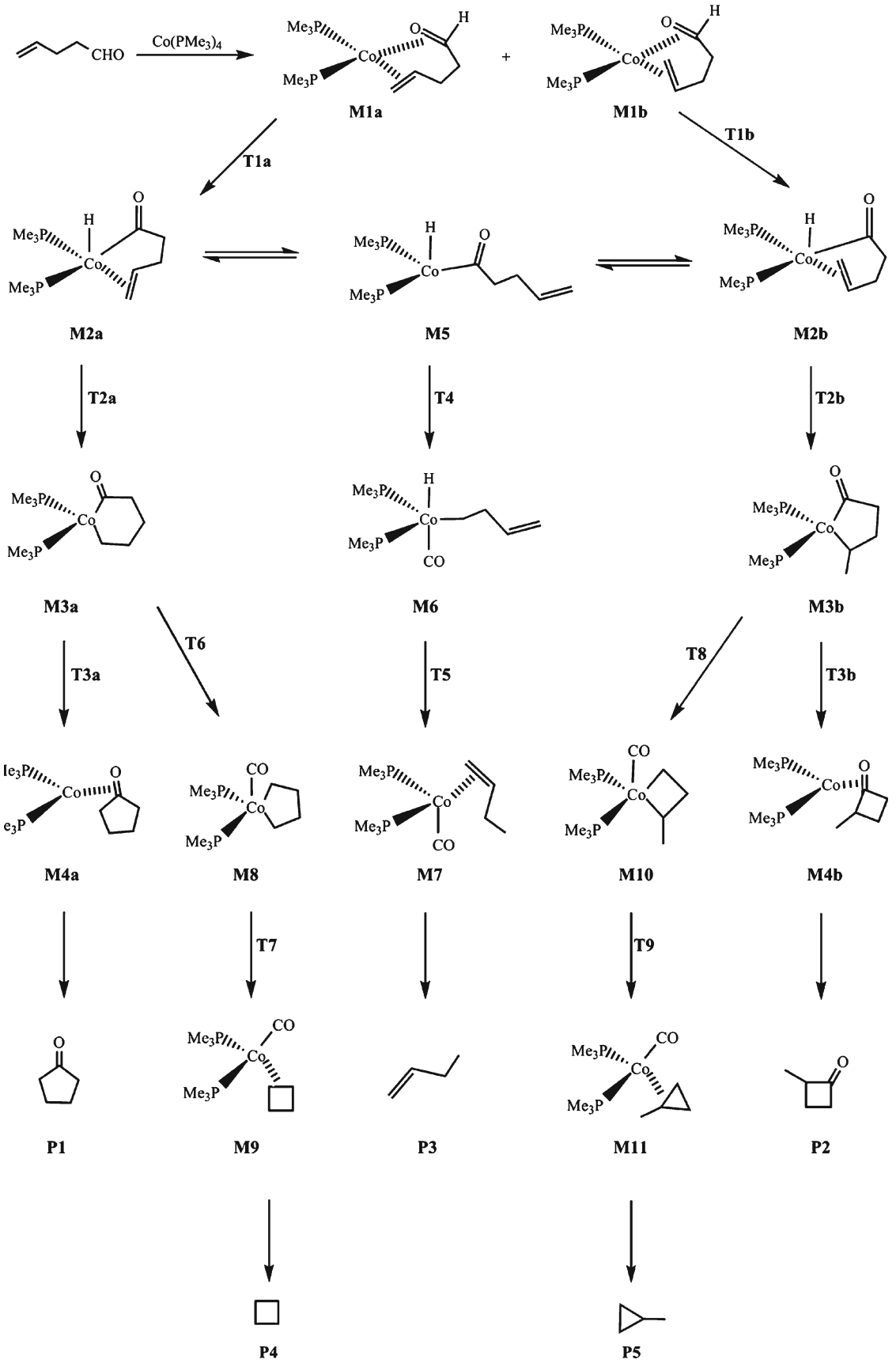

Scheme 2 Possible reaction mechanism of cobalt(0)-catalyzed intramolecular hydroacylation of 4-pentenal

Table 1 Reaction free energy barriers $\Delta G^{\neq}$(sol) (kJ mol^{-1}) (in THF) and $\Delta G^{\neq}$ (kJ mol^{-1}) (in gas phase), reaction enthalpy barriers $\Delta H^{\neq}$ (kJ mol^{-1}), and reaction energy barriers $\Delta E^{\neq}$ (kJ mol^{-1}) for all transition states

Transition state	$\Delta G^{\neq}$(sol)	$\Delta G^{\neq}$	$\Delta H^{\neq}$	$\Delta E^{\neq}$
T1a	68.4	77.2	71.7	72.4
T2a	49.2	48.4	49.2	50.1
T3a	50.3	50.4	48.8	50.3
T1b	43.4	52.5	50.9	51.5
T2b	17.2	8.3	11.2	11.3
T3b	83.0	78.9	76.7	77.7
T4	98.7	102.6	87.3	90.6
T5	33.9	29.6	32.1	31.9
T6	37.4	37.5	29.6	32.5
T7	187.9	176.0	181.2	180.1
T8	84.4	77.4	75.7	76.5
T9	107.4	102.2	104.2	103.8

bond was weakened greatly, as demonstrated by analyzing the change in bond order, P_{ij}, and electron density, ρ, at the BCPs (e.g., Co–H1 bond, P_{ij}, **M1a**: 0.001→**T1a**: 0.202→**M2a**: 0.284; ρ, **M1**: 0.000→**T1a**: 0.107→**M2a**: 0.122 e Å^{-3}). The high stabilization energies of 905.7, 485.5, 387.6, and 327.8 kJ mol^{-1} for the $\sigma_{C1-H1}\rightarrow\sigma^*_{Co-C1}$, $\sigma_{Co-C1}\rightarrow\sigma^*_{C1-H1}$, $\sigma_{C1-H1}\rightarrow\pi^*_{C1-O}$, and $(3\ s)_P\rightarrow(3d)^*_{Co}$, in **T1a** (Table S3, Supporting Information), which was obtained from the second-order perturbation analysis of donor–acceptor interactions in the NBO analysis and used to estimate the strengths of the donor–acceptor interactions of the NBOs, revealed the strong interaction between σ_{C1-H1} and σ^*_{Co-C1} or π^*_{C1-O}, σ_{Co-C1} and σ^*_{C1-H1}, $(3\ s)_P$ and $(3d)^*_{Co}$, the electron transfer tendency from σ_{C1-H1} to σ^*_{Co-C1} or π^*_{C1-O}, σ_{Co-C1} to σ^*_{C1-H1}, $(3\ s)_P$ to $(3d)^*_{Co}$. These results indicated that the C–H oxidative addition reaction was promoted. NBO analysis of **M2a** indicated that the Co–H1 and Co–C1 bonds showed strong single-bonded character, and NBO energies of the bonding orbitals σ_{Co-H1} and σ_{Co-C1} were −719 and −916 kJ mol^{-1}, respectively. In the intramolecular hydrometallation, because of different steric resistance in **M2a**, hydrogen migration had only one reaction channel. **T2a** involved a Co–C1–C2–C3–C4–C5 six-membered ring and a Co–H1–C4–C5 four-membered ring, and the electron densities of the RCPs were 0.023, 0.078 e Å^{-3}. Co–C1 and Co–C5 bonds of **M3a** were 1.836 and 1.961 Å, respectively, and NBO analysis indicated that both showed strong single-bonded character (NBO energies, σ_{Co-C1}: −990, σ_{Co-C5}: −800 kJ mol^{-1}). **T3a** involved a Co–C1–C5 three-membered ring and a C1–C2–C3–C4–C5 five-membered ring, and the electron densities of the RCPs were 0.082, and 0.028 e Å^{-3}, respectively.

Formation of cyclobutanone

Figure 3 showed the potential energy hypersurface for the pathway forming cyclobutanone. Intermediate **M1b** went through the oxidative addition reaction to form the five-coordinated complex **M2b**, via transition state **T1b** with a reaction free energy barrier of 43.4 kJ mol^{-1}. Next, **M2b** underwent a hydrogen transfer reaction through transition state **T2b** with a reaction free energy barrier of 17.2 kJ mol^{-1}, resulting in complex **M3b**. Finally, **M3b** underwent a reductive elimination reaction via transition state **T3b** with a reaction free energy barrier of 83.0 kJ mol^{-1} to yield the complex **M4b** generating the cyclobutanone **P2**. Clearly, the reductive elimination reaction was the rate-determining step for this reaction channel, which was different from those discussed above in the formation of cyclopentanone. The reaction free energy barrier of **T3b** was higher than that of **T1a** by 14.6 kJ mol^{-1}, so cyclopentanone **P1** was more dominant than cyclobutanone **P2**. Furthermore, Fig. 3 also shows that it is harder for complex **M3b** to form **M4b** than to revert back to **M1b**, because the free energy barrier is higher by 56.9 kJ mol^{-1}. Hence, the final product of the reaction channel was complex **M1b**, which could isomerize to the lower energy complex **M1a**.

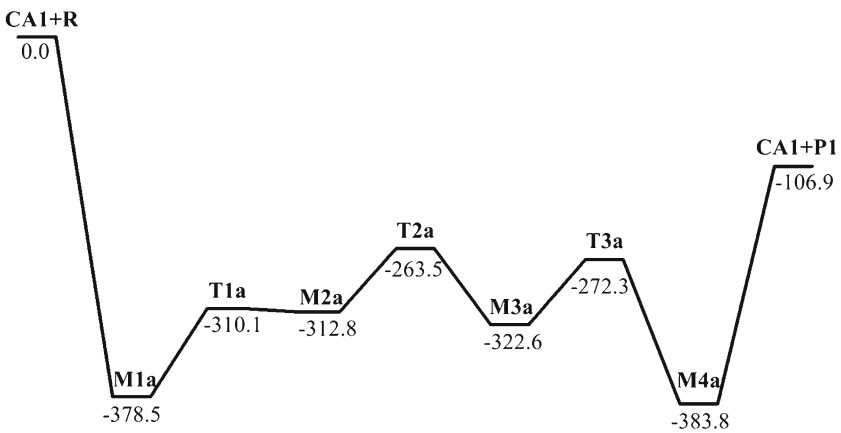

Fig. 1 Free energy profile for the proposed pathway forming cyclopentanone. Relative free energies ΔG(sol) in kJ mol^{-1}

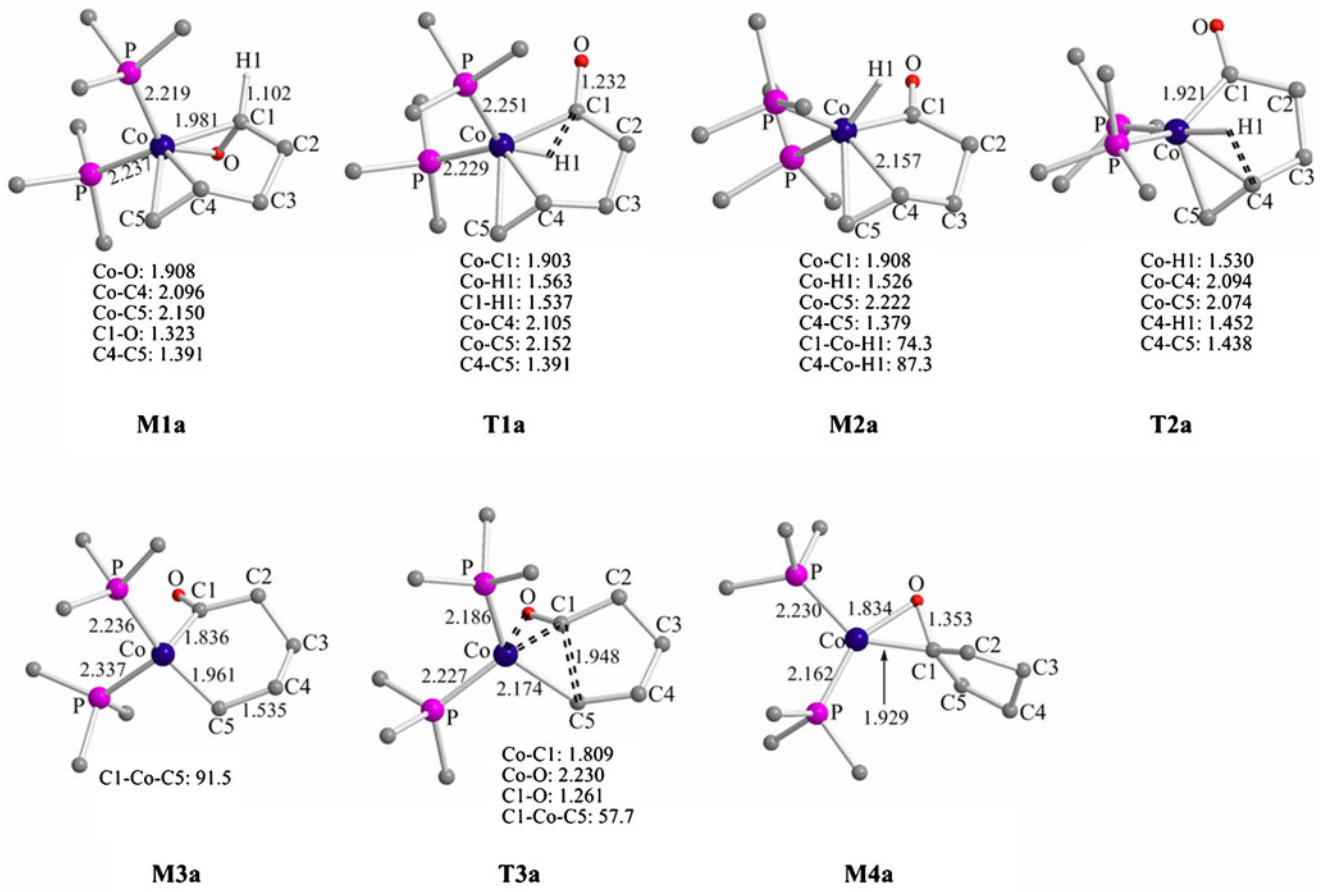

Fig. 2 Intermediates and transition states in the pathway forming cyclopentanone. Bond distances in Å, angles in degrees

As illustrated in Figs. 2 and 4, **T1b** has similar geometry and energy as that of **T1a**, and **M2b** shares similar geometry and energy with **M2a**. In the intramolecular hydrometallation, because of different steric resistance in **M2b**, hydrogen migration also had only one reaction channel. **T2b** involved a Co–C1–C2–C3–C4–C5 six-membered ring and a Co–H1–C5–C4 four-membered ring. NBO analysis of **M3b** indicated that Co–C1 and Co–C4 bonds showed strong single-bonded character (NBO energies, $\sigma_{Co\text{-}C1}$: −960, $\sigma_{Co\text{-}C4}$: −750 kJ mol^{-1}, which were higher than **M3a**.). **T3b** involved a Co–C1–C4 three-membered ring and a C1–C2–C3–C4 four-membered ring.

Formation of butylene

Figure 5 shows the potential energy hypersurface for the pathway forming butylene. Both intermediates **M2a** and **M2b** isomerize to a four-coordinated complex **M5**. Next, intermediate **M5** undergoes a decarbonylation reaction through transition state **T4** with a reaction free energy

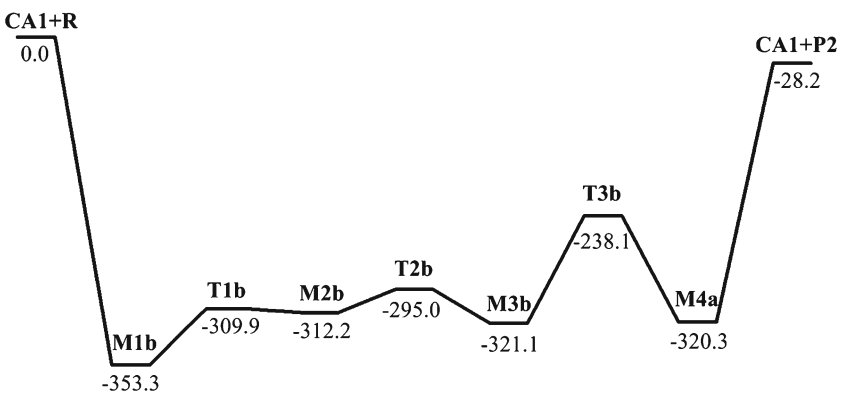

Fig. 3 Free energy profile for the proposed pathway forming cyclobutanone. Relative free energies ΔG(sol) in kJ mol^{-1}

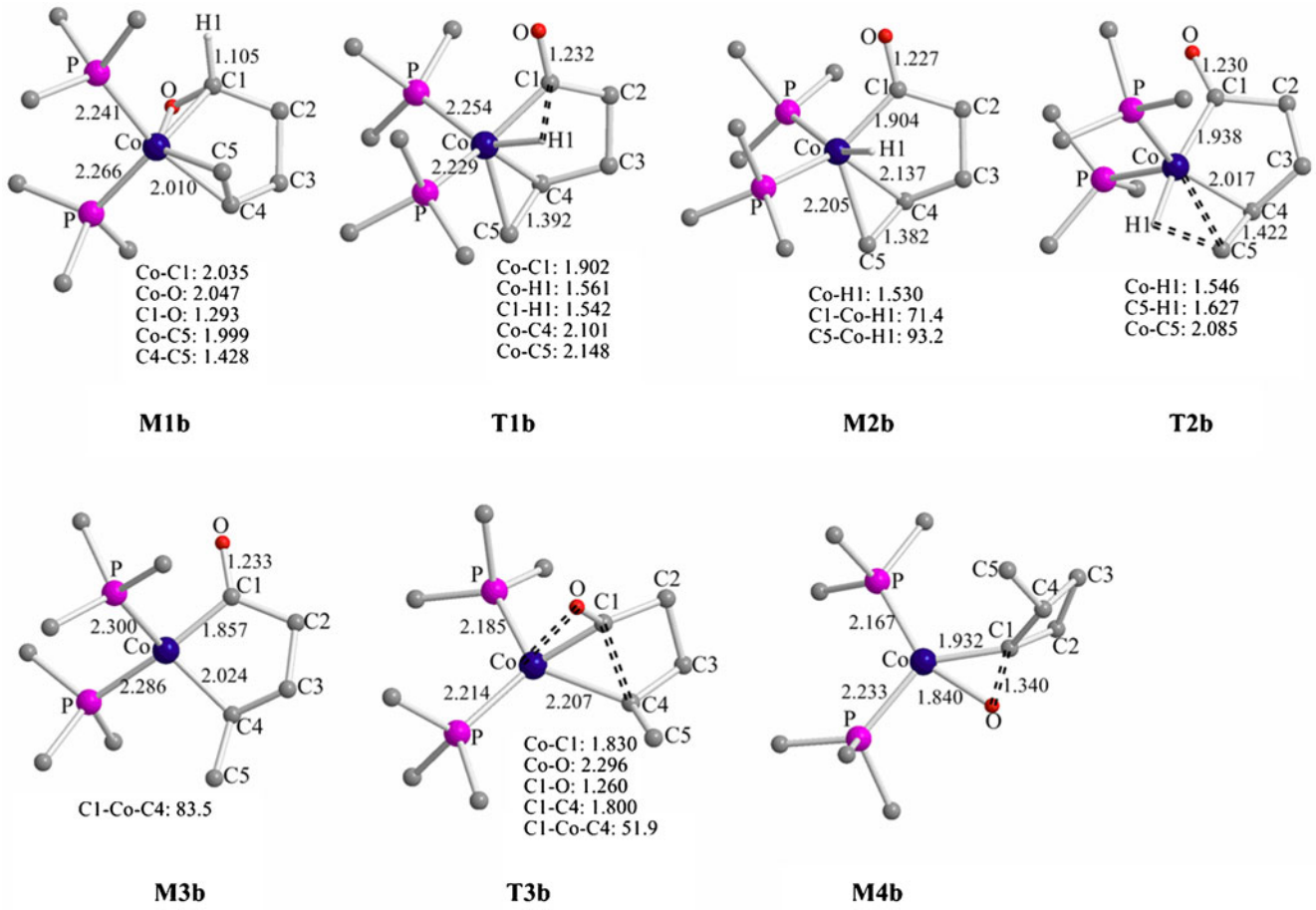

Fig. 4 Intermediates and transition states in the pathway forming cyclobutanone. Bond distances in Å, angles in degrees

barrier of 98.7 kJ mol^{-1}, leading to a five-coordinated complex **M6**. Finally, intermediate **M6** underwent hydrogen transfer reaction via transition state **T5** with a reaction free energy barrier of 33.9 kJ mol^{-1} to generate the complex **M7** giving the butylene **P3**. Obviously, the decarbonylation reaction was the rate-determining step for this reaction channel. The reaction free energy barrier of **T4** was higher than **T1a** by 30.3 kJ mol^{-1}, so cyclopentanone **P1** was more dominant than butylene **P3**.

Intermediate **M5** was a four-coordinated complex, and the Co–C1 bond was 1.853 Å (Fig. 6). NBO analysis of **M5** indicated that Co–C1 and Co–H1 bonds showed strong single-bonded character. Intermediate **M6** was a five-coordinated complex, and Co–H1, Co–C1, and Co–C2 bonds were 1.500, 1.798, and 2.015 Å. NBO analysis of **M6** indicated that Co–H1, Co–C1, and Co–C2 bonds showed strong single-bonded character.

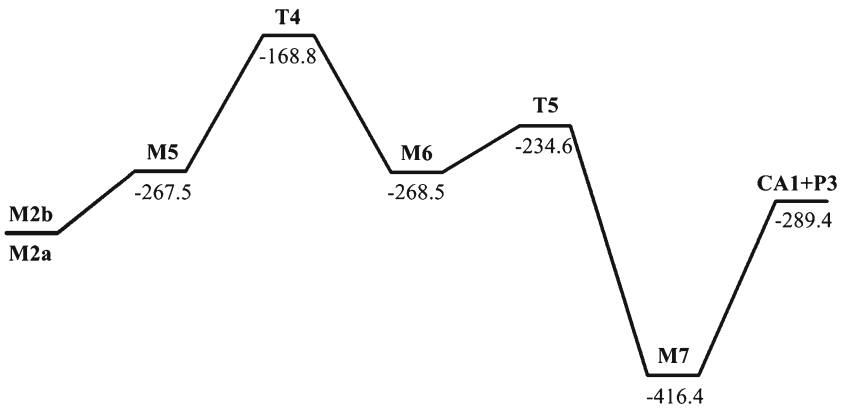

Fig. 5 Free energy profile for the proposed pathway forming butylene. Relative free energies ΔG(sol) in kJ mol^{-1}

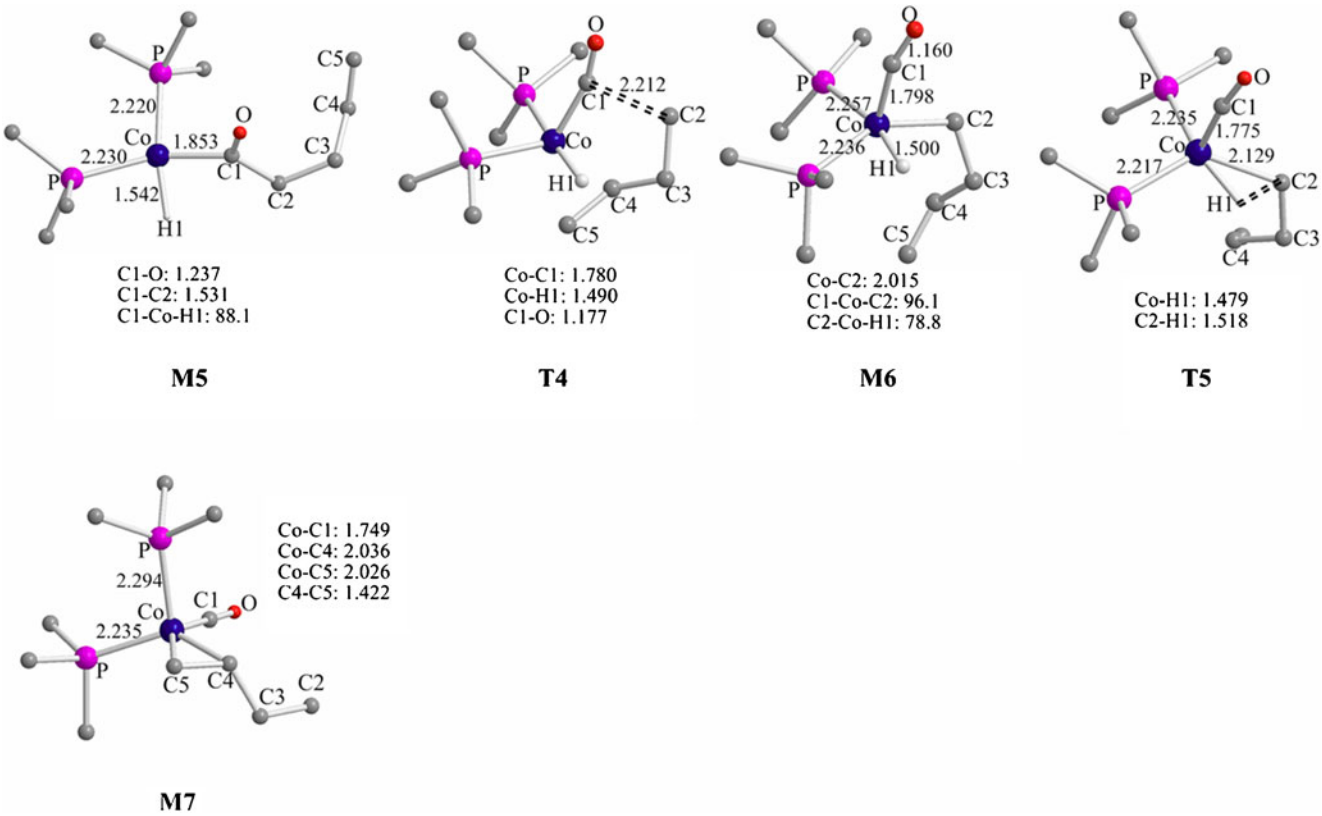

Fig. 6 Intermediates and transition states in the pathway forming butylene. Bond distances in Å, angles in degrees

Formation of cyclobutane

Figure 7 shows the potential energy hypersurface for the pathway forming cyclobutane. Intermediate **M3a** went through a decarbonylation reaction via transition state **T6** with a reaction free energy barrier of 37.4 kJ mol^{-1} to give the five-coordinated complex **M8**. Intermediate **M8** underwent a reductive elimination reaction through transition state **T7** with a reaction free energy barrier of 187.9 kJ mol^{-1} to form complex **M9** generating the cyclobutane **P4**. The reductive elimination reaction was clearly the rate-determining step for this reaction channel. The reaction free energy barrier of **T7** was higher than that of **T1a** by 119.5 kJ mol^{-1}, so cyclopentanone **P1** was more dominant than cyclobutane **P4**. Figure 7 also showed that it was harder for complex **M8** to give **M9** than to revert back to **M3a**, because of higher free energy barrier by 110.1 kJ mol^{-1}.

As illustrated in Fig. 8, Co–C1, Co–C2, and Co–C5 bonds of **M8** were 1.758, 2.043, and 2.033 Å, respectively. NBO analysis indicated that these bonds showed strong single-bonded character. Transition state **T7** involved a Co–C2–C5 three-membered ring and a C2–C3–C4–C5

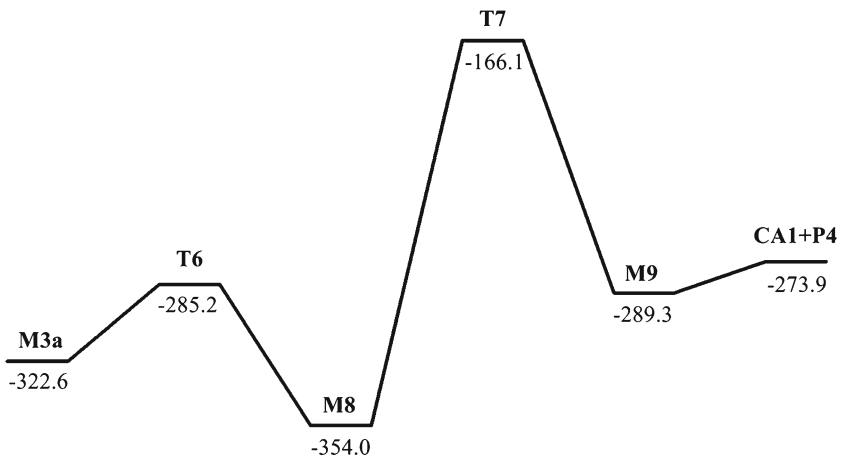

Fig. 7 Free energy profile for the proposed pathway forming cyclobutane. Relative free energies ΔG(sol) in kJ mol^{-1}

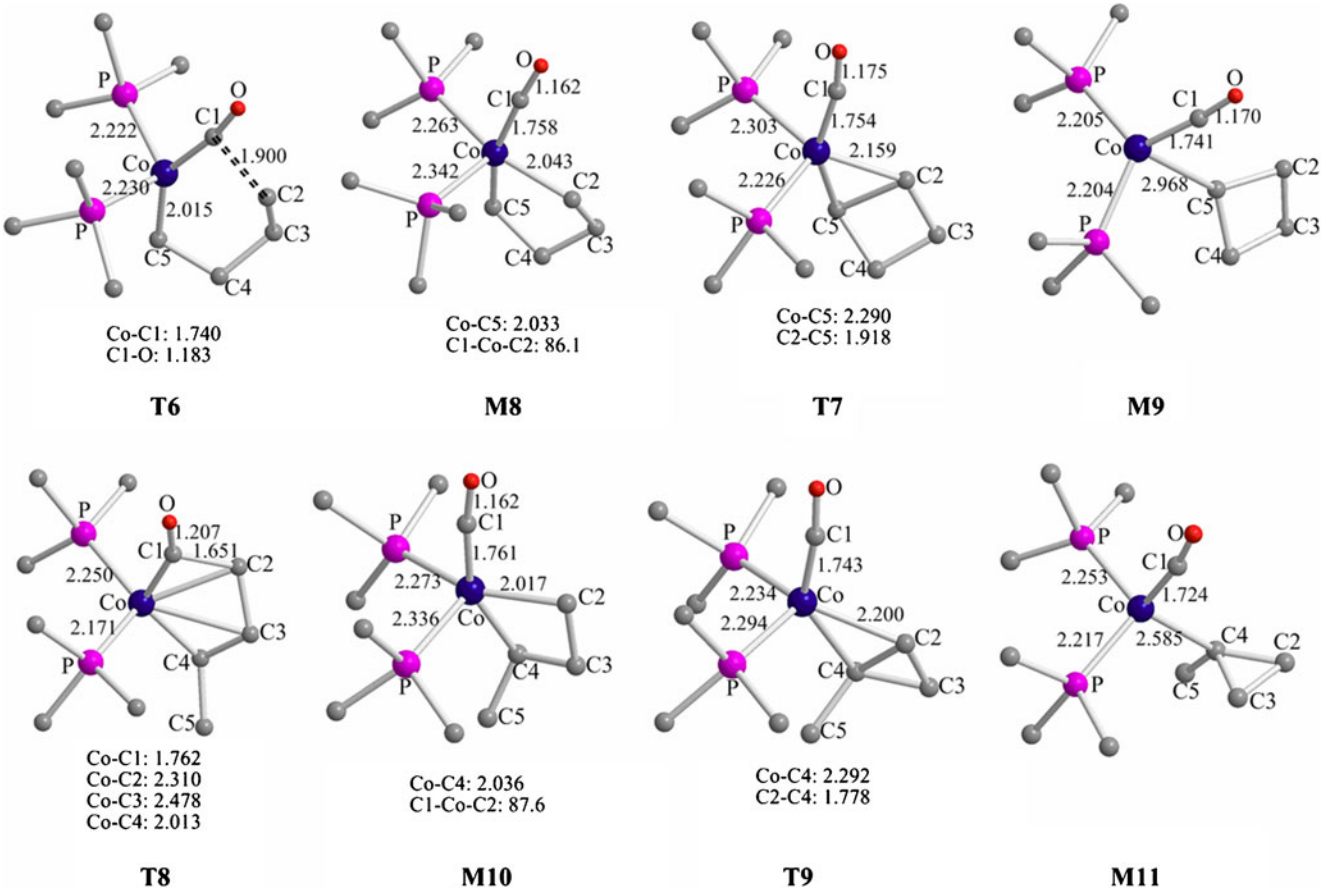

Fig. 8 Intermediates and transition states in the pathway forming cyclobutane and cyclopropane. Bond distances in Å, angles in degrees

four-membered ring, and Co–C1, Co–C2, and Co–C5 bonds were 1.754, 2.159, and 2.290 Å, respectively.

Formation of cyclopropane

Figure 9 shows the potential energy hypersurface for the pathway forming cyclopropane. Intermediate **M3b** underwent a decarbonylation reaction via transition state **T8** with a reaction free energy barrier of 84.4 kJ mol^{-1}, leading to the five-coordinated complex **M10**. Intermediate **M10** underwent a reductive elimination reaction through transition state **T9** with a reaction free energy barrier of 107.4 kJ mol^{-1} to give complex **M11** generating cyclobutane **P5**. Obviously, the reductive elimination reaction was the rate-determining step for this reaction channel. The reaction free energy barrier of **T9** was higher than that of **T1a** by 39.0 kJ mol^{-1}, so cyclopentanone **P1** was more dominant than cyclopropane **P5**.

Intermediate **M10** was a five-coordinated complex, and Co–C1, Co–C2, Co–C4 bonds were 1.761, 2.017, 2.036 Å,

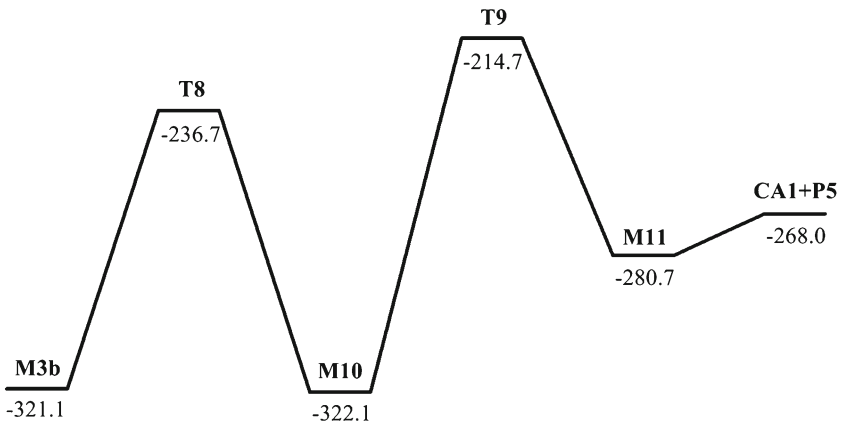

Fig. 9 Free energy profile for the proposed pathway forming cyclopropane. Relative free energies ΔG(sol) in kJ mol^{-1}

respectively (Fig. 8). Transition state **T9** involved two three-membered rings: Co–C2–C4 and C2–C3–C4, and Co–C1, Co–C2, Co–C4 bonds were 1.743, 2.200, 2.292 Å, respectively.

Overview of reaction mechanism

Possible reaction pathways were outlined in Scheme 2 above. We studied five such possible reaction pathways: the formation of cyclopentanone, cyclobutanone, butylenes, cyclobutane, and cyclopropane. The former two represent pathways of Co(0)-catalyzed intramolecular hydroacylation, while the latter three are pathways of decarbonylation.

In the reaction channel forming cyclopentanone, the oxidative addition reaction of 4-pentenal was the rate-determining step [a reaction free energy barrier $\Delta G^{\neq}(\mathrm{sol})_{\mathbf{T1a}}$ =68.4 kJ mol^{-1}]. In the channel forming cyclobutanone, the reductive elimination reaction was the rate-determining step [$\Delta G^{\neq}(\mathrm{sol})_{\mathbf{T3b}}$=83.0 kJ mol^{-1}]. In the channel forming butylenes, the decarbonylation reaction was the rate-determining step for this reaction channel [$\Delta G^{\neq}(\mathrm{sol})_{\mathbf{T4}}$=98.7 kJ mol^{-1}]. In the channel forming cyclobutane, the reductive elimination reaction was the rate-determining step [$\Delta G^{\neq}(\mathrm{sol})_{\mathbf{T7}}$= 187.9 kJ mol^{-1}]. In the channel forming cyclopropane, the reductive elimination reaction was the rate-determining step [$\Delta G^{\neq}(\mathrm{sol})_{\mathbf{T9}}$=107.4 kJ mol^{-1}]. Clearly, the formation of cyclopentanone was the most favorable reaction pathway, so cyclopentanone was the most dominant product, which was consistent with the experiments [19–21].

In addition, as illustrated in Figs. 3 and 9, it was clear that it was more difficult for complex **M3b** to form **M4b** or **M10** than to revert back to **M1b**, so the final product of two reaction channels was complex **M1b**, which could isomerize to the lower energy complex **M1a**. Figure 7 also shows that it was harder for complex **M8** to give **M9** than to revert back to **M3a**. Therefore, the formation of cyclopentanone was the most favorable reaction pathway (Figure S1, the black line), and the decarbonylation reaction was prohibited.

Conclusions

The reaction mechanisms of cobalt(0)-catalyzed intramolecular hydroacylation of 4-pentenal were explored computationally using DFT. The calculated results indicated that this reaction had five possible product types: cyclopentanone, cyclobutanone, butylenes, cyclobutane, and cyclopropane. Consistent with experiments, the first of these was the most dominant. So, the formation of cyclopentanone was the most favorable channel, and the oxidative addition reaction of 4-pentenal was the rate-determining step. Because of the much higher free energy barriers, the decarbonylation reaction was prohibited. Solvation had a significant effect, decreasing greatly the free energies of all intermediates and transition states.

Acknowledgment This work was supported by Natural Science Foundation of Shandong Province, P.R.C.

References

1. Jun CH, Lee JH (2004) Application of C–H and C–C bond activation in organic synthesis. Pure Appl Chem 76:577–587
2. Jia C, Kitamura T, Fujiwara Y (2001) Catalytic functionalization of arenes and alkanes via C–H bond activation. Acc Chem Res 34:633–639
3. Guari Y, Sabo-Etienne S, Chaudret B (1999) Catalytic formation of carbon–carbon bonds by activation of carbon–hydrogen bonds. Eur J Inorg Chem 1999:1047–1055. doi: 10.1002/(SICI)1099-0682(199907)1999:7<1047::AID-EJIC1047>3.0.CO;2-B
4. Arndtsen BA, Bergman RG, Mobley A, Peterson TH (1995) Selective intermolecular carbon–hydrogen bond activation by synthetic metal complexes in homogeneous solution. Acc Chem Res 28:154–162
5. Shilov AE, Shul'pin GB (1997) Activation of C–H bonds by metal complexes. Chem Rev 97:2879–2932
6. Dyker G (1999) Transition metal catalyzed coupling reactions under C–H activation. Angew Chem Int Ed 38:1698–1712
7. Ritleng V, Sirlin C, Pfeffer M (2002) Ru-, Rh-, and Pd-catalyzed C–C bond formation involving C–H activation and addition on unsaturated substrates: reactions and mechanistic aspects. Chem Rev 102:1731–1770
8. Labinger JA, Bercaw JE (2002) Understanding and exploiting C–H bond activation. Nature 417:507–514
9. Kakiuchi F, Murai S (2002) Catalytic C–H/olefin coupling. Acc Chem Res 35:826–834
10. Willis MC (2010) Transition metal catalyzed alkene and alkyne hydroacylation. Chem Rev 110:725–748
11. Willis MC, Randell-Sly HE, Woodward RL, McNally SJ, Currie GS (2006) Rhodium-catalyzed intermolecular chelation controlled alkene and alkyne hydroacylation: synthetic scope of β-S-substituted aldehyde substrates. J Org Chem 71:5291–5297
12. Imai M, Tanaka M, Nagumo S, Kawahara N, Suemune H (2007) Nitrile-promoted Rh-catalyzed intermolecular hydroacylation of olefins with salicylaldehyde. J Org Chem 72:2543–2546
13. Jun CH, Jo EA, Park JW (2007) Intermolecular hydroacylation by transition-metal complexes. Eur J Org Chem 2007:1869–1881
14. Roy AH, Lenges CP, Brookhart M (2007) Scope and mechanism of the intermolecular addition of aromatic aldehydes to olefins catalyzed by Rh(I) olefin complexes. J Am Chem Soc 129:2082–2093
15. Moxham GL, Randell-Sly H, Brayshaw SK, Weller AS, Willis MC (2008) Intermolecular alkene and alkyne hydroacylation with β-S-substituted aldehydes: mechanistic insight into the role of a hemilabile P–O–P ligand. Chem Eur J 14:8383–8397
16. Phan DHT, Kim B, Dong VM (2009) Phthalides by rhodium-catalyzed ketone hydroacylation. J Am Chem Soc 131:15608–15609
17. Shibata Y, Tanaka K (2009) Rhodium-catalyzed highly enantioselective direct intermolecular hydroacylation of 1,1-disubstituted alkenes with unfunctionalized aldehydes. J Am Chem Soc 131:12552–12553
18. Phan DHT, Kou KGM, Dong VM (2010) Enantioselective desymmetrization of cyclopropenes by hydroacylation. J Am Chem Soc 132:16354–16355

19. Vinogradov MG, Tuzikov AB, Nikishin GI (1985) Intramolecular hydroacylation catalyzed by cobalt complexes. Russ Chem Bull 34:325–329
20. Vinogradov MG, Tuzikov AB, Nikishin GI (1985) Intramolecular hydroacylation reaction catalyzed by $Co_2(N_2)(PPh_3)_6$ in the presence of various ligands. Russ Chem Bull 34:2369–2374
21. Vinogradov MG, Tuzikov AB, Nikishin GI (1989) Cyclization of unsaturated aldehydes catalyzed by $(PPh_3)_2Co(L2)$. Russ Chem Bull 38:2353–2356
22. Lenges CP, Brookhart M (1997) Co(I)-catalyzed inter- and intramolecular hydroacylation of olefins with aromatic aldehydes. J Am Chem Soc 119:3165–3166
23. Lenges CP, White PS, Brookhart M (1998) Mechanistic and synthetic studies of the addition of alkyl aldehydes to vinylsilanes catalyzed by Co(I) complexes. J Am Chem Soc 120:6965–6979
24. Lenges CP, Brookhart M, White PS (1999) Structure and reactivity of a cobalt(I) phthalaldehyde complex with both σ- and π-bonded aldehyde groups. Angew Chem Int Ed 38:552–555
25. Tsuda T, Kiyoi T, Saegusa T (1990) Nickel(0)-catalyzed hydroacylation of alkynes with aldehydes to α, β-enones. J Org Chem 55:2554–2558
26. Taniguchi H, Ohmura T, Suginome M (2009) Nickel-catalyzed ring-opening hydroacylation of methylenecyclopropanes: synthesis of γ, δ-unsaturated ketones from aldehydes. J Am Chem Soc 131:11298–11299
27. Fukuyama T, Doi T, Minamino S, Omura S, Ryu I (2007) Ruthenium hydride catalyzed regioselective addition of aldehydes to enones to give 1,3-diketones. Angew Chem Int Ed 46:559–5561
28. Omura S, Fukuyama T, Horiguchi J, Murakami Y, Ryu I (2008) Ruthenium hydride-catalyzed addition of aldehydes to dienes leading to β, γ-unsaturated ketones. J Am Chem Soc 130:14094–14095
29. Hatanaka S, Obora Y, Ishii Y (2010) Iridium-catalyzed coupling reaction of primary alcohols with 2-alkynes leading hydroacylation products. Chem Eur J 16:1883–1888
30. Hyatt IFD, Anderson HK, Morehead AT Jr, Sargent AL (2008) Mechanism of rhodium-catalyzed intramolecular hydroacylation: a computational study. Organometallics 27:135–147
31. Chung LW, Wiest O, Wu YD (2008) A theoretical study on the trans-addition intramolecular hydroacylation of 4-alkynals catalyzed by cationic rhodium complexes. J Org Chem 73:2649–2655
32. Gao JG, Wang F, Meng QX, Li M (2008) Density functional computations of Rh(I)-catalyzed hydroacylation of ethene or ethyne. J Theor Comput Chem 7:1041–1053
33. Meng QX, Shen W, Li M (2012) Mechanism of intermolecular hydroacylation of vinylsilanes catalyzed by rhodium(I) olefin complex: a DFT study. J Mol Model 18:1229–1239
34. Frisch MJ, Trucks GW, Schlegel HB, Scuseria GE, Robb MA, Cheeseman JR, Montgomery JA, Vreven JT, Kudin KN, Burant JC, Millam JM, Iyengar SS, Tomasi J, Barone V, Mennucci B, Cossi M, Scalmani G, Rega N, Petersson GA, Nakatsuji H, Hada M, Ehara M, Toyota K, Fukuda R, Hasegawa J, Ishida M, Nakajima T, Honda Y, Kitao O, Nakai H, Klene M, Li X, Knox JE, Hratchian HP, Cross JB, Adamo C, Jaramillo J, Gomperts R, Stratmann RE, Yazyev O, Austin AJ, Cammi R, Pomelli C, Ochterski JW, Ayala PW, Morokuma K, Voth GA, Salvador P, Dannenberg JJ, Zakrzewski VG, Dapprich S, Daniels AD, Strain MC, Farkas O, Malick DK, Rabuck AD, Raghavachari K, Foresman JB, Ortiz JV, Cui Q, Baboul AG, Clifford S, Cioslowski J, Stefanov BB, Liu G, Liashenko A, Piskorz P, Komaromi I, Martin RL, Fox DJ, Keith T, Al-Laham MA, Peng CY, Nanayakkara A, Challacombe M, Gill PMW, Johnson B, Chen W, Wong MW, Gonzalez C, Pople JA (2004) Gaussian 03, Revision D.02. Gaussian, Inc, Wallingford
35. Parr RG, Yang W (1989) Density-functional theory of atoms and molecules. Oxford University Press, New York
36. Becke AD (1993) Density-functional thermochemistry. III. The role of exact exchange. J Chem Phys 98:5648–5652
37. Lee C, Yang W, Parr RG (1988) Development of the Colle-Salvetti correlation-energy formula into a functional of the electron density. Phys Rev B 37:785–789
38. Gonzalez C, Schlegel HB (1990) Reaction path following in mass-weighted internal coordinates. J Phys Chem 94:5523–5527
39. Flükiger P, Lüthi HP, Portmann S, Weber J (2000–2002) MOLEKEL 4.3 Swiss Center for Scientific Computing. Manno, Switzerland
40. Portmann S, Lüthi HP (2000) An interactive molecular graphics tool. Chimia 54:766–770
41. Carpenter JE, Weinhold F (1988) Analysis of the geometry of the hydroxymethyl radical by the "different hybrids for different spins" natural bond orbital procedure. J Mol Struct (THEOCHEM) 169:41–50
42. Foster JP, Weinhold F (1980) Natural hybrid orbitals. J Am Chem Soc 102:7211–7218
43. Reed AE, Weinstock RB, Weinhold F (1985) Natural population analysis. J Chem Phy 83:735–746
44. Reed AE, Curtiss LA, Weinhold F (1988) Intermolecular interactions from a natural bond orbital, donor-acceptor viewpoint. Chem Rev 88:899–926
45. Glendening ED, Badenhoop JK, Reed AE, Carpenter JE, Bohmann JA, Morales CM, Weinhold F (2001) NBO 5.0. Theoretical Chemistry Institute, University of Wisconsin, Madison
46. Marten B, Kim K, Cortis C, Friesner RA, Murphy RB, Ringnalda MN, Sitkoff D, Honig B (1996) New model for calculation of solvation free energies: correction of self-consistent reaction field continuum dielectric theory for short range hydrogen-bonding effects. J Phys Chem 100:11775–11788
47. Friesner RA, Murphy RB, Beachy MD, Ringnalda MN, Pollard WT, Dunietz BD, Cao YX (1999) Correlated ab initio electronic structure calculations for large molecules. J Phys Chem A 103:1913–1928
48. Miertus S, Tomasi J (1982) Approximate evaluations of the electrostatic free energy and internal energy changes in solution processes. Chem Phys 65:239–245
49. Bader RFW (1990) Atoms in molecules, a quantum theory. International Series of Monographs in Chemistry, vol 22. Oxford University Press, Oxford
50. Biegler-König F, Schönbohm J, Derdau R, Bayles D, Bader RFW (2002) AIM 2000. Version 2.0, McMaster University, Hamilton, ON, Canada